Free-Wake Analysis of Compressible Rotor Flows

John Steinhoff* and K. Ramachandran†
University of Tennessee Space Institute, Tullahoma, Tennessee

A method for computing helicopter rotor flowfields is described that is fully compressible, and which computes the wake without requiring external specification of any flow quantity. Also, it is unified, treating the blade and wake regions as a single domain. It is quite different from most compressible treatments which require that the regions be treated separately. The method has been developed into a computer program, "HELIX I," for the computation of compressible rotor flowfields in hover with free wakes. Results of this program are also described. The method utilizes a generalization of a compressible finite-volume potential flow scheme. This scheme has been extensively used in the fixed-wing industry for research and wing design, and has been shown to be effective for resolving shocks and to be in good agreement with experiment for subsonic and transonic flows. We obtain similar agreement for rotor flowfield solutions, as shown by computed surface pressure plots. In addition, with our new wake treatment, we are able to compute wake positions that are in substantial agreement with experiment. Cases treated include subsonic and transonic flows, high- and low-aspect ratios, and two- and four-bladed rotors.

I. Introduction

MOST current methods for computing rotor flowfields including wakes are based on integral or finite-difference techniques.[1] Integral methods, in the form of lifting-line or lifting-surface methods, are able to treat the rotor blade as well as the wake in a single unified way.[2] They, however, have several disadvantages: restriction to linear, low-speed shock-free cases; difficulty attaining stable solutions, particularly in hover, where a large number of interacting vortex sheets must be treated; incapable of treating the flow on the blade accurately; and, finally, the computation time increases rapidly with the number of elements used to represent the blade/vortex system (as the square). The most serious limitation is the low-speed restriction, since modern rotor blades operate in the transonic regime, where compressibility is important, and shocks can exist in the flow.

Finite-difference methods, on the other hand, usually can treat compressibility effects and can accurately solve for the flow in the immediate region of the blade. Most of these methods, which include potential flow and Euler-based methods, however, when applied to rotor flows, do not treat the flowfield in a single unified way: they isolate the region close to each blade and only solve the difference equations in that region. The entire vortex system is treated using a different technique, such as a classical lifting-line or lifting-surface method. This vortex calculation is used to determine an induced velocity on the surface of the finite-difference grid surrounding each blade, which is then used as a boundary condition for the finite-difference calculation in a coupled iteration scheme.

An exception to the above methods is the technique described here. This method, like the above finite-difference ones, is fully compressible and can resolve transonic effects such as shocks. Unlike the others, however, it treats the entire relevant flow region, including the blades and vortex sheets, in a unified way. This entire region is discretized, as in a solution for a fixed-wing case, and only far-field boundary conditions are used at the (distant) computational boundaries. In this way, solutions can be developed without concern as to whether the computed vortex sheet lies outside of a special artificial region about each blade.

A reason that conventional Euler-equation schemes may not be suitable for such a unified approach is that they attempt to solve for the internal structure of the sheet, as well as its motion, whereas this internal structure is modeled in our method. With Euler methods, accurate computation of a concentrated vortex sheet is most effective very close to the blade since numerical viscosity spreads the sheet as it is convected.[3]

Also, a reason that such a unified method is not feasible with conventional potential methods is that they treat the vortex sheets as discontinuities in the potential. Such a treatment constrains the sheets to lie on segments of surfaces of the computational grid. Accordingly, in conventional potential methods, only short segments of the sheets, which are fairly flat, and where the grid can be distorted to follow the sheet, can be accurately treated. This results, as in Euler methods, in a restriction to small regions near each blade.[4]

Instead of the above ways of treating the vortex sheets, we embed them in a compressible potential flowfield. The potential is defined on a set of grid points, as in standard methods. Also, as in these methods, the mass balance relations are enforced at each point on the grid. The potential, however, does not have any discontinuities, and therefore does not represent any vorticity. The vorticity is represented by a separate velocity field which is added to the gradient of the potential. This added field is concentrated in sheets, as is the vorticity that results from it. No external specification of the strength of these sheets or their location is required. These are determined by the computed flowfield in a coupled iterative way by requiring the sheet to follow the mean flow. Thus, it is a true free-wake vortex method. The internal structure of the sheet is modeled, however, and not solved for on the grid. Since this structure is of a smaller length scale than the other features of the problem, it is very economical to use such an approach. Conversely, since it is actually determined by turbulent viscous

Presented as Paper 87-0542 at the AIAA 25th Aerospace Sciences Meeting, Reno, Nevada, Jan. 12-15, 1987; received July 23, 1987; revision received Feb. 10, 1989.

*Associate Professor, Department of Engineering Science and Mechanics. Member AIAA.

†Research Scientist, Flow Analysis, Inc.

effects, to accurately compute this thin, internal region with a finite-difference scheme as it convects through the flow would be very costly.

Upon convergence, the total velocity field satisfies mass conservation on a fixed grid, as in conventional Euler or potential flow methods. Unlike potential methods with fixed wakes, however, momentum is conserved everywhere, although with a different numerical approximation than in conventional Euler methods. Away from the wake, or vortex sheet, the flow, which obeys the irrotational, isentropic full potential equation there, satisfies momentum conservation, since, for the flows of interest, shocks are not very strong and there is no significant entropy or vorticity production. Through the wake, due to its proper treatment, momentum is also conserved. This would not be true if the wake were treated as a flat sheet, as in conventional potential-flow methods.

Initial uses of the method for a vortex line convecting past a wing in compressible flow were published in 1983.[5] A preliminary use of the method for rolling-up vortex sheets was also published in 1983.[6]

In this paper, results will be presented for flow over both two-blade and four-blade rotors, including a transonic case. Where data is available, these results will be compared with experiments. The computed solutions presented are results of a computer code, HELIX I, which implements the methods described for rotor flowfields in hover. Some of the two-blade results were presented in Refs. 7 and 8.

II. Basic Method

A. Iteration Scheme

Our basic approach involves modifying the potential-flow wake treatment so that, within the numerical approximation, momentum is conserved there, as in the rest of the field. The internal structure of the vortex is not solved for, but is modeled and spread over several grid points. The wake position and vorticity strength are computed so that momentum over the wake is balanced in an integral sense. Using momentum equations in the form of vorticity transport, streamlines outside the wake which have no vorticity upstream must not cross the wake where there is vorticity. Thus, the wake remains sandwiched between sets of irrotational streamlines, extending downstream from above and below the rotor blade trailing edge. This defines the wake position. The vorticity within the wake is defined by the requirements of vorticity conservation and pressure balance, which also result from the momentum equations. This formulation allows the internal structure of the wake, which is largely determined by viscous effects, to be specified, if it is important to do so. This internal structure, which has a much smaller scale than other features of the flow, is not solved for by the finite-difference method, and large numbers of grid points need not be dedicated to resolving it. Also, as in flows with shocks or axially symmetric straight vortex lines, it may be true that the internal structure has little influence on the flow outside the internal regions, as long as overall conservation laws are enforced. Then, even very crude, ad hoc internal profiles may be used.

We first decompose the velocity into a freestream, potential, and vortical part:

$$q = \Omega \times r + \nabla\phi + q^v \tag{1}$$

The vortical part q^v is concentrated near the sheet. A fixed grid (in the rotating blade-fixed frame) is used to solve the compressible potential-flow equation for the potential ϕ:

$$\partial_x(\rho u) + \partial_y(\rho v) + \partial_z(\rho w) = 0 \tag{2}$$

where ρ is the density and has the isentropic form away from the sheet based on the total velocity q with components u, v, and w.

$$\rho = \left\{1 - \left(\frac{\gamma - 1}{2}\right) M_\infty^2[(\Omega \times r)^2 - q^2]\right\}^{\frac{1}{\gamma - 1}}$$

The vortical component q^v is spread over several grid points around the vortex sheet so that vorticity is concentrated there.

During iteration towards convergence (the solution is steady in the blade coordinate system for hover), a four-step procedure is repeatedly used.

1) The vortex sheet position is integrated as a set of marker streamlines to follow the flow using interpolated values of q from the fixed grid.

2) q^v is computed at grid points near the sheet.

3) A potential ϕ is computed at each grid point to satisfy Eq. (2), with q^v fixed.

4) A new velocity q is computed at each grid point based on Eq. (1).

At convergence Eq. (2) is satisfied and the vortex sheet follows the flow.

Although the vortex sheet is effectively spread over several grid points, there is no cumulative numerical diffusion and the spreading remains fixed at its input value. Thus, the *internal* structure of the sheet is modeled rather than computed. As opposed to prescribed wake methods, in our method the *wake system* is not modeled but solved for, while only the internal structure is modeled. Also, experimental or theoretical information can, if desired, be inserted into the method to prescribe this internal structure, while no experimental information is needed for the wake position. This is similar to boundary-layer methods which are used for flow over wing surfaces and coupled to potential-flow methods. It will be seen that good results can be obtained with a very crude internal structure model requiring no inputs from experiment or parameter adjustments to fit data.

B. Vortical Velocity Calculation

Once a set of marker locations is known, the vortical velocity at any location r can be computed. A simple method uses the following relation:

$$q^v(r) = C\sum\Gamma_l\, \sigma(|r - r_l|)q_l^v \tag{3}$$

where Γ_l is the circulation at the trailing edge where the particular marker (l) originated, the spreading function,

$$\sigma(\Delta r) = \max\left(0, 1 - \frac{(\Delta r)^2}{a^2}\right) \tag{4}$$

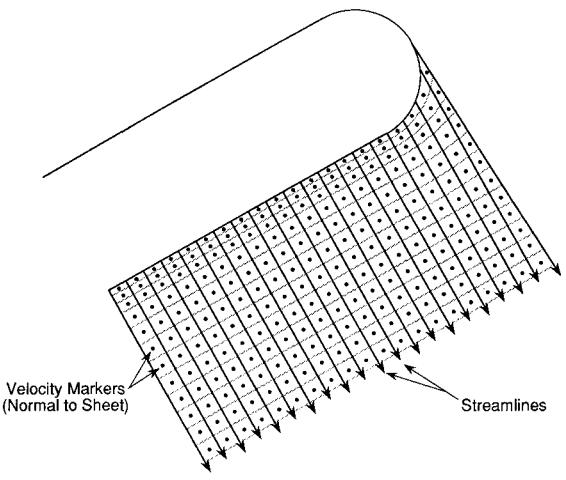

Fig. 1 Three-dimensional velocity markers.

and q_l^v is a vector normal to each panel and proportional to the panel area (see Fig. 1). The normalization constant C is such that, in the limit when the markers are closely spaced and Γ_l is slowly varying, the integral of $q^v(r)$ through the sheet at any marker (m) equals Γ_m. The only quantity specified is a, the spreading distance, which is taken to be about three cell widths. Stable, smooth solutions have been found using this spreading. Reducing a below about two cell widths often results in irregularities in the solution. A second representation was also used. This particularly simple and accurate form for q^v involves a Clebsch-type of representation:

$$q^v = \Gamma^c \nabla \psi \tag{5}$$

where $\Gamma^c(r)$ is a three-dimensional field which smoothly goes to the appropriate Γ (circulation value) on the sheet as r approaches the sheet surface. The potential $\psi(r)$ smoothly goes from $+1/2$ on one side of the sheet to $-1/2$ on the other. A convenient formula for $\psi(r)$ is

$$\psi(r) = \tfrac{1}{2}\sin(\pi S_n), \qquad |S_n| < a/2 \tag{6a}$$

$$\psi(r) = +1/2, \qquad S_n > +a/2 \tag{6b}$$

$$\psi(r) = -1/2, \qquad S_n < -a/2 \tag{6c}$$

where S_n is a (signed) normal distance from the point r to the sheet, and a is again a specified spreading distance.

We use interpolation-like formulas similar to Eq. (3) to compute $\Gamma^c(r)$ and $S_n(r)$ at any grid point r:

$$\Gamma^c(r) = \left[\sum_\ell \Gamma_\ell \sigma(\Delta r_\ell)\right]/A \tag{7a}$$

$$S_n(r) = \left[\sum_\ell S_\ell^n(r, r_\ell)\sigma(\Delta r_\ell)\right]/A \tag{7b}$$

$$A = \sum_\ell \sigma(\Delta r_\ell) \tag{7c}$$

$$\Delta r_\ell = r - r_\ell \tag{7d}$$

where $S_\ell^n(r, r_\ell)$ is a normal vector from r to a tangential plane through the sheet at marker ℓ, and the sign of S_n depends on which side of the sheet r is on. Even though ψ is nonzero throughout the field (except on the sheet), $\nabla\psi$ is zero beyond the spreading distance from the sheet. Accordingly, both $\Gamma^c(r)$ and $\psi(r)$ need be computed only on those grid points that are in a narrow band about the sheet with thickness of the order of the spreading distance. Another very important property of this q^v is the elimination of spurious numerical vorticity in regions near the sheet where Γ is constant (no physical vorticity on the sheet). In such regions, $\Gamma^c(r)$ will be constant and q^v can be written as

$$q^v = \nabla[\Gamma^c \psi(r)] \tag{8}$$

Even though q^v is still nonzero, if the same numerical differencing scheme is used for $\nabla\psi$ as is used for $\nabla\phi$, the effect of the sheet in regions of zero vorticity will be identically zero. This is not true for our first formulation of q^v given by Eq. (3). This resulted in a requirement for larger spreading distances and thicker vortices (for a given grid) with the earlier method.

It is important to realize that only short-range q^v, such as given above, can be efficient for use in our scheme. If we had a long-range form, given, for example, by the Biot-Savart law, then the q^v calculation would have to be made for each point in the entire grid. Each of these calculations would effectively involve a two-dimensional integration over the entire vortex sheet. This part of the calculation would then be prohibitively expensive.

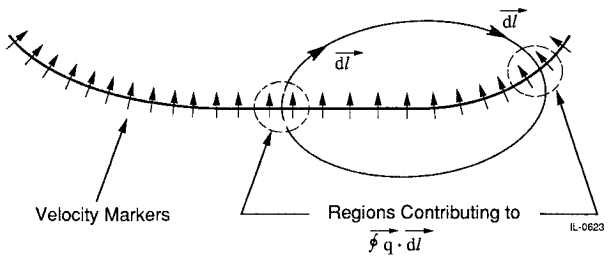

Fig. 2 Circulation integral.

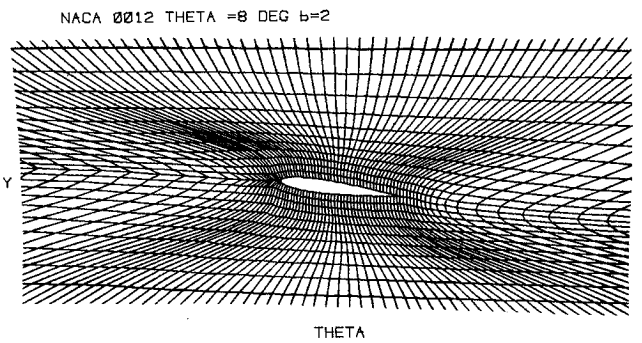

Fig. 3 Inner portion of grid.

Since the vortex sheet represents a rapid tangential velocity change, it might be expected that q^v should be tangential to the sheet and not normal to it. However, referring to Fig. 2, a plane approximately normal to the vorticity in the sheet, we can see that q^v must be normal if it is to be short-range. The closed line integral of $q \cdot dl$ around a portion of the sheet is equal to the area integral of ω_n through the closed path, where ω_n is the component of vorticity normal to the plane of the figure. Since $\nabla\phi$ does not contribute to the line integral and q^v is short-range, only those portions of the line near the sheet, encircled by dashed curves, contribute to the integral. In these regions only a normal velocity will contribute, and so q^v must have a normal component. It can also be seen with this argument that vorticity is conserved. No matter how q^v is distributed along the sheet within the closed curve, the area integral of ω_n is determined by the two small areas where the path crosses, which are equal to the circulation corresponding to the markers at those points.

The motion of the markers through the velocity field is determined by the requirement that the integral of momentum through the sheet be conserved. Then, streamlines initially above or below the sheet do not cross it and the pressure above and below the sheet is balanced. This latter requirement means that, since the flow is isentropic outside the sheet, the magnitude of the velocity on both sides must be equal. Both of these requirements are approximately satisfied by requiring the markers to follow the mean of the two velocities.

C. Potential Calculation

During each iteration of the cycle described in Sec. IIA, a rapid approximation factorization "AFZ" method is used to solve the conservative, finite-volume potential-flow equations (with q^v fixed). These equations have been used extensively for fixed-wing calculations and their solutions have been shown to agree well with experiment even in cases with moderate shocks. This is described more fully in Refs. 5 and 9. The factorization is used in two-dimensional cylindrical surfaces about the rotor axis. A grid on one of these surfaces is shown in Fig. 3 as a function of angle about the axis and height, for a typical blade profile. Only the inner part of the grid near the blade is shown. The angular extent depends on the number of blades present. The grid is periodic at the two vertical edges and the potential and q^v are also forced to be periodic there. For q^v, this just

means that when a marker leaves the downstream edge it reappears at the same height and radius at the upstream edge.

The grid is a particular type of "H" mesh with the singularity at the leading edge analytically removed. This type of grid was investigated in detail for two-dimensional transonic flows,[10] and shown to give accurate results when used with the finite-volume potential-flow equations. A simple blending technique[11] was used to enforce the outer and periodic boundary conditions on the grid.

The upper boundary is at about a half-rotor span. Dirichlet conditions are imposed on the potential there, using a form given in Ref. 12 for a semiinfinite vortical cylinder, which approximates the vortex system at this boundary. At the lower boundary, about 0.8 span below the rotor disk, a corrected periodic condition is imposed on both q^v and the potential. In this region, the markers are descending at an approximately constant rate and the vortex sheet is approximately periodic in height (y). If this vortex system were infinite, then the velocity would be periodic: a correction is required since the vortex system is only semiinfinite. The correction involves adding a velocity similar to that used at the upper boundary.

At the blade surface, the normal velocity is zero, which implies

$$\partial_n \phi = -q_n^v \tag{9}$$

Finally, Dirichlet conditions are used at the outer cylindrical boundary and, for simplicity, Neumann conditions are used on an inner cylinder inside the root.

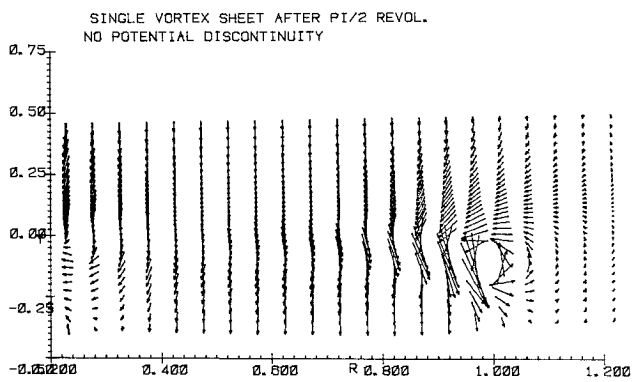

Fig. 4 Crossflow—constant THETA.

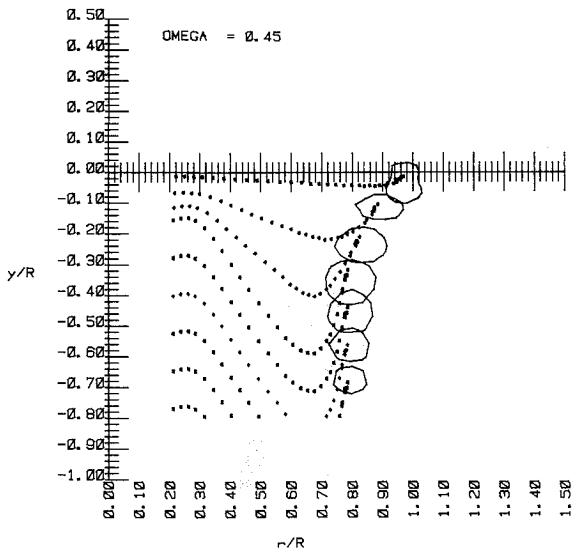

Fig. 5 Individual sheet vorticity contours.

III. Results

Results are presented for the full solution of a lifting rotor in hover, as computed by the three-dimensional compressible flow code, HELIX I. Previous results of the method, published elsewhere, described a line vortex propagating past a three-dimensional wing,[5] and a vortex sheet rolling up in a parabolized approximation.[6] Figures 4–14 present results using the first version of our method, which involves Eq. (3). In Fig. 4, preliminary results of the full three-dimensional compressible code are presented for a single vortex sheet shed by a rotor blade. Here, the velocity in a cross plane normal to the motion behind the trailing edge is presented. The cross-stream velocity clearly shows a tight vortex which is the size specified by the model used (Gaussian distribution). This remains the same size as it is convected downstream. Other internal vortex structures and density distributions consistent with the grid spacing could also be imposed. For this case, an untwisted Joukowski profile was used with a pitch of 5 deg and an aspect ratio of 19.

Figure 5 depicts the computed sheet position (defined by markers) 35 deg after passage of the blade (positions of sheets 5–7 are extrapolated to reduce computing time), for the above Joukowski blade. Also, Fig. 5 depicts vorticity contours for the separate contribution of each individual sheet for relative values of 0.45 (in the same plane). The contour value is chosen to show the effects of the individual sheets as well as the spreading.

Figures 6 and 7 present computed results for a two-blade rotor with an aspect ratio of 18.2, constant NACA0012 cross section, no twist, pitch of 8 deg, and a tip Mach number of 0.61. These conditions match the experimental ones published in Ref. 13. The computed vertical motion and contraction of the tip vortex (calculated at the centroid of the computed vortex sheet) are presented and compared with experimental results of Ref. 13. The comparison is seen to be fairly close,

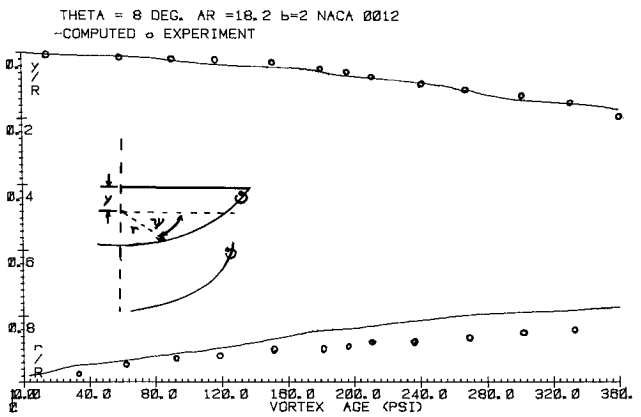

Fig. 6 Tip-vortex geometry (Mtip = 0.61).

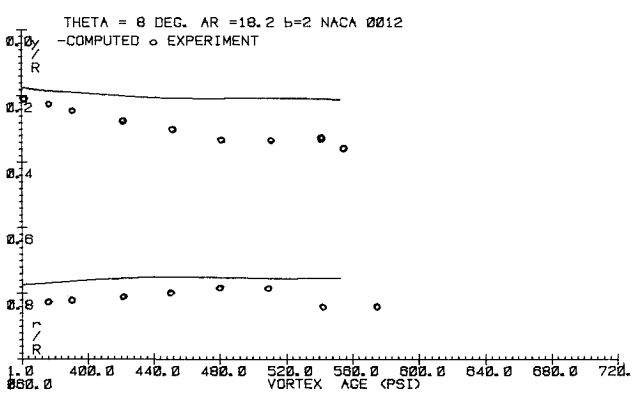

Fig. 7 Tip-vortex geometry (Mtip = 0.61).

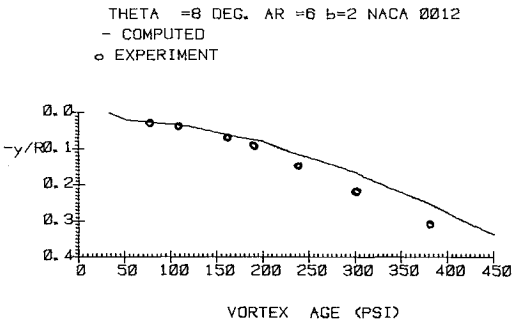

Fig. 8 Tip-vortex geometry (Mtip = 0.436).

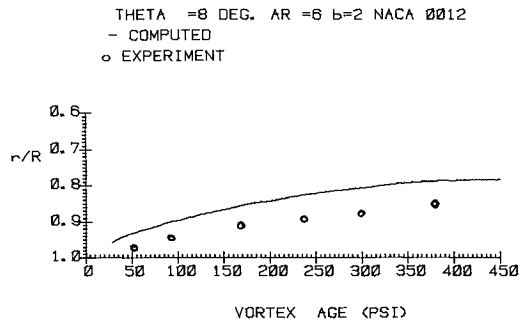

Fig. 9 Tip-vortex geometry (Mtip = 0.436).

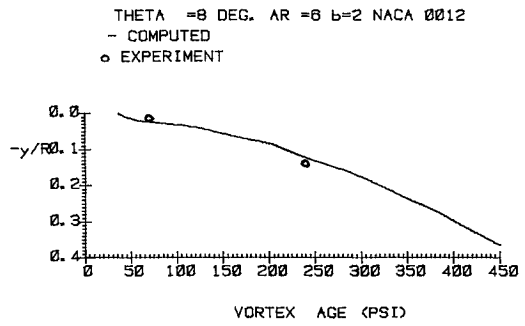

Fig. 10 Tip-vortex geometry (Mtip = 0.877).

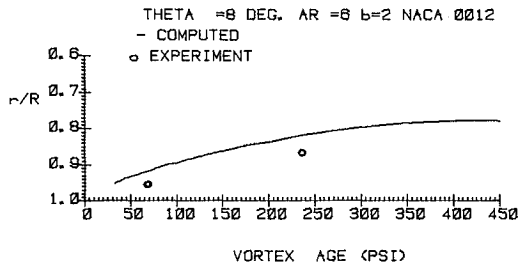

Fig. 11 Tip-vortex geometry (Mtip = 0.877).

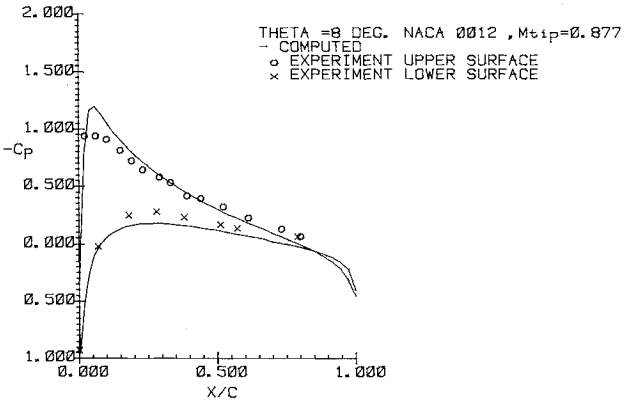

Fig. 12 Chordwise-pressure distribution (Mtip = 0.877, $r/R = .68$).

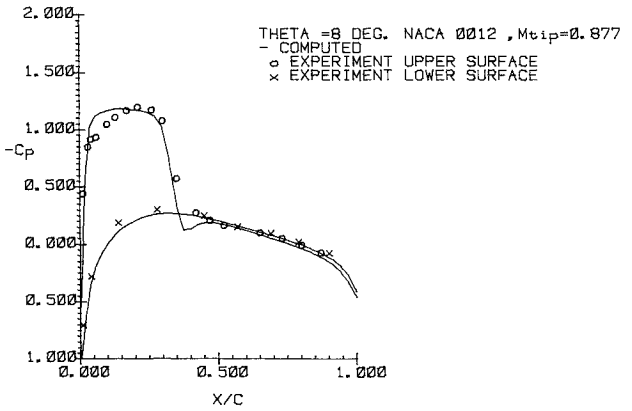

Fig. 13 Chordwise-pressure distribution (Mtip = 0.877, $r/R = .89$).

even though no adjustable parameters were used in the calculation.

In Figs. 8 and 9, the vortex geometry is presented for the same blade and pitch, but with aspect ratio of 6.0 and tip Mach number of 0.436. The experimental vortex geometry of Ref. 14 for the same case is also presented. The agreement is seen to be fairly good.

Another two-blade case involved the same rotor with a (transonic) tip Mach number of 0.877. The computed vortex vertical motion is presented in Fig. 10 and contraction in Fig. 11. In Figs. 12–14, computed C_p values are presented for r/R values of 0.68, 0.89, and 0.96, respectively. These results are also compared with the experimental data of Ref. 14. The comparison can be seen to be good except for the C_p values in the 0.96 case, which is very close to the tip. To resolve this region, a finer grid is required there. Also, the relatively coarse grid used near the tip results in a vortex width there which is larger than experiment (although this width does not increase as the vortex convects). This can be seen in Figs. 7, 9, and 11 where the vortex centroid does not start at the tip of the rotor, but slightly inboard.

These calculations were done with the initial formulation of the method. Even though good results were obtained for two-blade rotors, a crucial test for HELIX I was the four-blade rotor, since there the vortex from each blade passes much closer to the preceding blade.

It can be shown that, as the grid is refined, the vortex spreading with this formulation, based on Eq. (3), must decrease less rapidly than the cell size. Otherwise, numerical effects appear which can be reflected in the motion of the vortex. The new formulation, based on Clebsch decomposition, should not have this problem. The discrepancies in the vortex descent rate between computation and experiments, visible in Figs. 6, 8, and 10, appear to have this numerical origin.

Some results for four-blade rotors obtained using the new formulation are presented below. Additional four-blade results and a more thorough discussion are presented in Ref. 8.

One case computed involved a NACA0012 profile with an aspect ratio of 18.2, -8 deg linear twist, pitch at 0.75 span equal to 8 deg, and tip Mach number 0.46. This corresponded to an experiment described in Ref. 13. The computed tip vortex descent is presented in Fig. 15 and contraction in Fig. 16. Also in Fig. 15, the two experimentally measured slopes, k_1 and k_2, for the descent before and after first-blade passage are represented. The experimentally measured vortex radii are presented in Fig. 16. Agreement with experiment is seen to be very good.

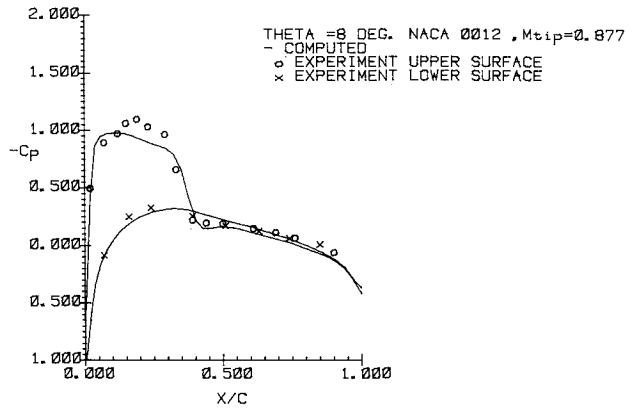

Fig. 14 Chordwise-pressure distribution (Mtip = 0.877), $r/R = .96$).

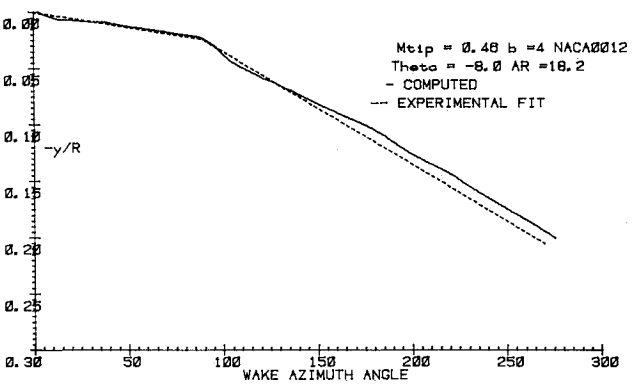

Fig. 15 Tip-vortex coordinates (axial).

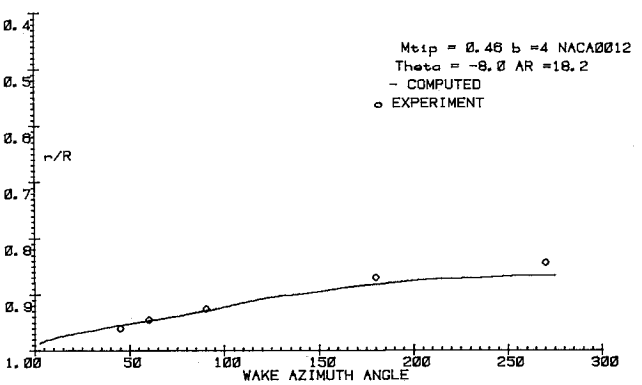

Fig. 16 Tip-vortex coordinates (radial).

IV. Conclusion

A method has been described to compute the three-dimensional flow over a helicopter rotor in hover, including compressibility and wake effects. The method requires no external data or parameter adjustments to define the wake position or other features of the flow. Only the blade geometry and rotational speed are required as inputs. The method has been implemented in a code, HELIX I. Results presented indicate good agreement with experiment for wake descent and contraction, as well as surface pressure distributions and thrust coefficients. These results include both high- and low-aspect ratio cases with two and four blades, and subsonic and transonic flows, including shocks.

Acknowledgment

This work was supported by Army Research Office (ARO) Contract DAAG29-K0019.

References

[1]Johnson, W., "Recent Developments in Rotary-Wing Aerodynamics," *AIAA Journal,* Vol. 24, Aug. 1986, pp. 1219–1244.

[2]Kocurek, J. D. and Tangler, J. L., "A Prescribed Wake Lifting Surface Hover Performance Analysis," The 32nd Annual National Forum of the American Helicopter Society, American Helicopter Society, Alexandria, VA, May, 1976.

[3]Aggarwal, R. and Deese, J., "Euler Calculations for Flowfield of a Helicopter Rotor in Hover," AIAA 4th Applied Aerodynamics Conference, San Diego, CA, June 1986.

[4]Egolf, T. A., and Sparks, S. P., "Hovering Rotor Airload Prediction Using a Full Potential Flow Analysis with Realistic Wake Geometry." The 41st Annual Forum of the American Helicopter Society, Ft. Worth, TX, May, 1985.

[5]Steinhoff, J., Ramachandran, K., and Suryanarayana, K., "The Treatment of Convected Vortices in Compressible Potential Flow," (AGARD-CPP-342) April 1983, p. 22-1.

[6]Steinhoff, J., and Suryanarayana, K., "The Treatment of Vortex Sheets in Compressible Potential Flow," *Proceedings of the Computational Fluid Dynamics Conference,* AIAA, New York, July 1983, p. 1.

[7]Steinhoff, J., and Ramachandran, K., "Free-Wake Analysis of Compressible Rotor Flowfields in Hover," Paper No. 20, Twelfth European Rotorcraft Forum, Garmisch-Partenkirchen, Federal Republic of Germany, Sept. 1986.

[8]Steinhoff, J., "A Vortex Embedding Method for Free-Wake Analysis of Helicopter Rotor Blades in Hover," Paper 2-11, Thirteenth European Rotorcraft Forum, Arles, France, Sept. 1987.

[9]Chow, R., Melnik, R., Marconi, F., and Steinhoff, J., Grumman Aerospace Corp., Bethpage, NY, RM-749, Aug. 1982.

[10]Pelz, R., and Steinhoff, J., *Proceedings of the ASME Winter Meetings on Computers in Flow Predictions and Fluid Dynamics Experiments,* American Society of Mechanical Engineering, New York, p. 27-33.

[11]Steinhoff, J., "Blending Method for Grid Generation," *Journal of Computational Physics,* Vol. 65, No. 2, Aug. 1986, pp. 370–385.

[12]Roberts, T. W., "Computational of Potential Flows with Embedded Vortex Rings and Applications to Helicopter Rotor Wakes," NASA-CR-166542, 1983.

[13]Landgrebe, A. J., "An Analytical and Experimental Investigation of Helicopter Rotor Hover Performance and Wake Geometry Characteristics," U.S. Army Airmobility Research and Development Lab., Moffett Field, CA, USAAMRDL TR 71-24, June 1971.

[14]Caradonna, F. X. and Tung, C., "Experimental and Analytical Studies of a Model Helicopter Rotor in Hover," NASA-TM-81232, 1981.